DETECTION OF 3D FILAMENTOUS NETWORKS FROM TOMOGRAPHIC ELECTRON MICROSCOPY

Leandro A. Loss[⋆] *Hang Chang*[⋆] *Purbasha Sarkar*[†] *Manfred Auer*[†] *Bahram Parvin*[⋆]

[⋆]Life Sciences Division, Lawrence Berkeley National Laboratory, Berkeley, CA, USA
[†]Energy Biosciences Institute, University of California, Berkeley, CA, USA

ABSTRACT

This paper presents a computational approach for detection of filamentous networks in 3D tomographic electron microscopy. Due to the general heterogeneity of chemical staining, imaged signatures may appear punctate and discontinuous. Very often, there is a necessity to characterize organization and phenotypic signatures of stained structures. This is the example of polysaccharides in the plant cell wall, where characterization of its inner structure allows for studies of their mechanical properties and accessibility. Our approach consists of three steps: (i) Hessian filtering for signal enhancement; (ii) tensor voting for detection and completion of organized patterns; and (iii) curve tracking for segmentation of filaments and junctions. We validated our approach by detecting filaments in synthetic images and real plant cell walls imaged by 3D tomographic electron microscopy.

Index Terms— Filament Segmentation, Perceptual Organization, Electron Microscopy, Plant Cell Wall

1. INTRODUCTION

Our goal is to develop an automatic framework for detection of filamentous networks imaged through tomographic electron microscopy. Such tool allows for quantitative analysis of heterogeneous data sets, whose structural signatures are hard to compute due to limitations of chemical staining and imaging technology. For example, there is a need to develop an analytical pipeline for comparative analyses and characterization of spatial organization of the filamentous formation within the plant cell wall. Considered a viable solution to the shortage of fossil fuels and their impact in climate changes, plant biomass has been identified as a source of large-scale biofuel production since the cell wall harbor energy-rich polysaccharides. If efficiently utilized and broken down into sugars, these polysaccharides can be fermented into ethanol and other transportation fuels.

Research supported by (i) the Energy Biosciences Institute, U.C. Berkeley (EBI grant No. 007G18), (ii) the National Cancer Institute (grant No. R01CA140663) under Contract No. DE-AC02-05CH11231, and (iii) the National Institute of Health (grant No. 2 P01 GM051487-15).

The main barriers in this enterprise are non-uniform foreground staining, variations in background signature, presence of noise, and perceptual arrangement of the polysaccharides (cellulose, pectin and hemi-cellulose). These barriers inhibit the use of standard methods (e.g., thresholding, skeletonization) for detecting and tracing filaments. Our approach relies on perceptual grouping, which aims to detect local features and to enforce continuity to construct a global representation. This achieved by the tensor voting paradigm [1]. Tensor voting is based on entities that deform under the influence of their vicinity to reveal perceptual structures. Since it depends on interaction from voxel to voxel, tensor voting can be very time-demanding when applied to a dense (i.e., not thresholded) 3D image. Here, Tensor Voting is coupled with Hessian filtering in order to function more efficiently, both in running time and quality of microfibril inference. Once filaments have been detected and perceptual gaps have been bridged, our curve tracking algorithm traces lines along filaments and detects junctions, providing a rich representation of the plant cell wall. We demonstrate the utility of our approach through real 3D electron tomograms of plant cell walls.

Previous attempts on imaging cell wall architecture have employed (i) transmission electron microscopy (TEM) of fast-frozen, deep-etched, rotary-shadowed replicas of cell walls [2]; (ii) field emission scanning electron microscopy (FESEM) of chemically extracted, freeze-fractured cell walls [3]; and (iii) atomic force microscopy (AFM) of fully hydrated cell walls [4]. Although they have provided an interesting insight on the in situ microfibril dimensions and orientations, as well as the degree of connections between the cell wall components, the information obtained is typically restricted to two dimensions or is topographical in nature. As to this date, electron tomography is the only method that has provided three-dimensional insight of plant cell walls at molecular resolution (e.g., [5]). However, tomography studies of plant cell walls have been restricted to chemically treated, severely extracted secondary cell walls from wood; and their analysis has been limited to small volumes of the wall. This is due, in part, to the limitation in manual segmentation, which is extremely labor-intensive for cell walls tightly packed with filamentous structures as small as 2 to 3 nm in diameter. Therefore, the development of an automatic

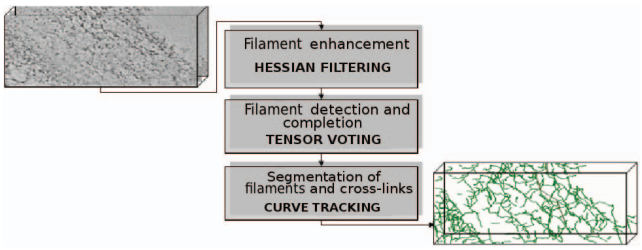


Fig. 1. Our approach detects filamentous networks from electron tomographic 3D data sets through a three-step computational protocol. As depicted in this diagram, Hessian filtering, tensor voting and curve tracking are coupled together to produce high quality segmentations of filamentous structures.

protocol for segmentation of filamentous structures in 3D tomographic electron microscopy is highly valuable.

In the remainder of this paper, Section 2 provides a description of the proposed approach. Section 3 describes our results in synthetic data and real plant cell walls. Section 4 concludes this manuscript with an overall view of the approach and achieved results, as well as future directions.

2. OUR APPROACH

Here we present our approach to segmentation of plant cell wall filamentous structures in 3D electron tomograms. The segmentation is achieved through a three-step approach, as depicted in Figure 1. First, Hessian filtering enhances filamentous regions by computing a second-order differential operator. Second, dense tensor voting is applied for detection of filaments and junctions, also bridging gaps for filament completion. Finally, curve tracking is employed and the filaments and junctions are segmented.

2.1. Enhancing Filamentous Structures

The first step of our approach utilizes a second order differential operator (i.e., Hessian) to enhance locations where filamentous structures are present. The approach is based on the fact that filamentous structures form an organized network of continuous, elongated fragments, and the encounter of 2 or more filaments form a junction. Previous works (e.g., [6] discuss the suitability of Hessian filtering for segmentation of curvilinear structures. The similarity among these works is the interpretation of the eigenvalues and eigenvectors of the processed image for structure inference. An image can be filtered using Equation 1, $\frac{\partial^2 I}{\partial\bullet\partial\circ} = \frac{\partial}{\partial\bullet}(\frac{\partial I}{\partial\circ})$, $\frac{\partial I}{\partial\circ} = \sigma I \times \frac{\partial}{\partial\circ}G(\sigma)$, and $G(\sigma)$ is a Gaussian function with standard deviation σ. The term σI promotes scale normalization.

$$H(I(x,y,z)) = \begin{bmatrix} \frac{\partial^2 I}{\partial x^2} & \frac{\partial^2 I}{\partial x \partial y} & \frac{\partial^2 I}{\partial x \partial z} \\ \frac{\partial^2 I}{\partial y \partial x} & \frac{\partial^2 I}{\partial y^2} & \frac{\partial^2 I}{\partial y \partial z} \\ \frac{\partial^2 I}{\partial z \partial x} & \frac{\partial^2 I}{\partial z \partial y} & \frac{\partial^2 I}{\partial z^2} \end{bmatrix} \quad (1)$$

For structural analysis, the result of Hessian filtering $H(I(x,y,z))$ is decomposed into eigenvalues ($|\lambda_1| \geq |\lambda_2| \geq |\lambda_3|$) and respective eigenvectors ($\overrightarrow{e}_1, \overrightarrow{e}_2, \overrightarrow{e}_3$). Here, we apply Hessian for enhancement of structures in the plant cell wall that are evidenced by chemical staining. In order to enhance filamentous structures and junctions that shows as bright signal against the dark non-stained background, we compute a probability map based on the highest absolute valued eigenvalue, $|\lambda_1|$. Locations where the highest eigenvalue is positive (dark structures) are zeroed and locations where the highest eigenvalue is negative (bright structures) are inverted to reflect a higher probability of structure. In addition, eigenvectors associated with the lowest eigenvalues ($\overrightarrow{e}_3$) define the tangential direction of filaments. Therefore, the probability map computed at this step is composed of a measure of *likelihood of bright structure*, $P_{H(x,y,z)}$, and a local estimate of *structure direction*, $\overrightarrow{P}_{H(x,y,z)}$.

2.2. Detecting and Completing Filaments

The next step of our approach explores the probability map computed from Hessian filtering to locate filamentous filaments and bridge any possible gaps. This is done by Tensor Voting [1]. In Tensor Voting, structural saliency is estimated through vote casting between primitives of an image. Such primitives are represented by tensors, mathematical entities whose capability for encoding magnitude and orientation make tensor voting particularly efficient for detection of perceptually organized structures, such as edges, lines and regions. In 3D, tensors are represented analytically as second order non-negative definite matrices or geometrically as ellipsoids, shaped by the tensors' eigenvalues' magnitude and eigenvectors' directions. Initialized with a certain size, shape and orientation, input tensors are gradually deformed due to the accumulation of votes cast by other neighboring tensors.

Votes are also tensors composed of magnitude and orientation, and encode the Gestalt principles of proximity, smoothness and good continuation. Given two tensors at locations (x,y,z) and (u,v,w), as depicted in Fig. 2(a), the relative distance l between them and the angle θ between the tangent of the osculating circle, of center C, at (x,y,z) and the imaginary planar line between (x,y,z) and (u,v,w) are used to calculate the primitives' relative arc length $s = \theta l/sin(\theta)$ and curvature $\kappa = 2sin(\theta)/l$. Together, they produce $V(u,v,w)$, (x,y,z)'s vote to (u,v,w), as shown by Equation 2.

$$V(u,v,w) = e^{-\frac{s^2 + c\kappa^2}{\sigma^2}} \overrightarrow{t}\,\overrightarrow{t}^T \quad (2)$$

In the expression above, $\overrightarrow{t}$ is the vector tangent to the osculating circle at location (u,v,w). It can be calculated by $[cos(2\theta) \quad -sin(2\theta)]^T$. The scale factor σ is the only free parameter in this expression and determines the extension of the voting neighborhood. The parameter $c = -16log(0.1) \times$

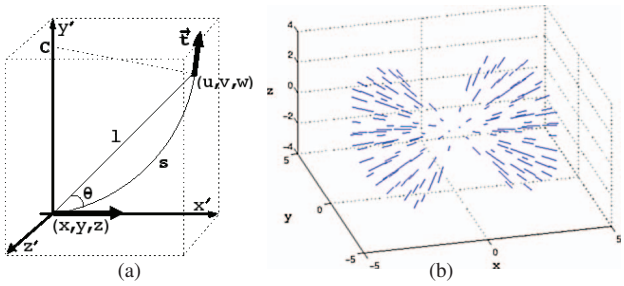


Fig. 2. (a) Illustrative example of tensors and their relationship to produce the vote $V(u, v, w)$ from equation 2. (b) Tensor voting stick field for voting along tangents.

$(\sigma - 1) \times \pi^{-2}$ and controls the decay at high curvature areas. A voting field can be formed by calculating all votes that can be cast from a tensor located in the center of the field to its neighboring tensors (Fig. 2(b)). Its extension is limited by σ, and it can only exist at $|\theta| \leq 45°$.

Lastly, voting can be either *sparse* or *dense*. The former restricts tensors to vote only on other encoded input tensors, while the latter allows tensors to vote everywhere within their neighborhood. Dense voting allows for inference of structures beyond the input map, bridging gaps, for instance.

2.3. Segmenting Filaments and Junctions

In our next step, 3D curve tracking allows for segmentation of filaments and junctions. Our curve tracking algorithm is based on concatenation of voxels with maximum local saliency $(\lambda_1 - \lambda_2)$ in the tensor voting saliency map. Our algorithm iterates through three basic steps: (i) search for an "unvisited" voxel with high saliency to initiate voxel concatenation; (ii) find concatenation candidates from tensor's main direction and its perpendicular vicinity; (iii) concatenate voxel with highest saliency among candidates. Concatenation stops when the saliency of the next to-be-concatenated voxel decays below a threshold T_{local}, producing a curve that underlies a filament. These steps repeat until the global saliency of unused voxels decay below a threshold T_{global}. Junctions are detected from delineated filaments that intersect one another during tracking.

3. EXPERIMENTS AND RESULTS

Our computational approach was designed to detect and delineate filamentous structures in full 3D images. To this end, we first validated our approach against synthetic data composed of a helix centered in images with different characteristics: noise (n) and missing elements (m). Next, we prepared a set of 3D electron tomograms of plant cell wall samples to provide a real scenario for evaluation of our automatic framework. We imaged plant cell walls from fully grown wild type Arabidopsis thaliana using (i) the Leica EM AMW automatic microwave tissue processor, (ii) the Leica EM U26 ultramicrotome for sample sectioning, (iii) a gold labeled dual axis tilt series [7], and (iv) IMOD for alignment and reconstruction of 3D tomograms [8]. Our data set consists of three replicates obtained by this methodology.

In the results reported here, Hessian filtering is first applied to the original tomogram with $\sigma = 4$. A probability map is built from the negative eigenvalues, as explained in Section 2. Tensor voting is then applied. The first step in applying tensor voting is to construct a voting space. We started by encoding every voxel from the Hessian probability map as an oriented tensor (a stick). Analytically speaking, $\lambda = [P_{H(x,y,z)} \;\; 0 \;\; 0]^T$, and $\overrightarrow{e} = \overrightarrow{P}_{H(x,y,z)} \overrightarrow{P}^T_{H(x,y,z)}$. After the voting space is constructed, a dense tensor voting pass is executed using the stick tensor field (Fig. 2(b)). Here, directions estimated by Hessian filtering are used to direct the votes cast from each location. Note that the tensor voting field is broad enough to accommodate imprecisions on the initial estimates. Also, locations that are thresholded out from the Hessian probability map (i.e., positive highest eigenvalue) encode tensors with $\lambda_1 = 0$ and do not cast votes. However, those locations may still receive votes, which enables us to bridge perceptual gaps. The deformation caused by locally accumulating votes from the stick tensor voting pass reveals, although still inaccurately, the presence or not of perceptual structures in the image. The resulting tensor's magnitude $(\lambda_1, \lambda_2, \lambda_3)$ and direction $(\overrightarrow{e}_1, \overrightarrow{e}_2, \overrightarrow{e}_3)$ are obtained by computing its eigen-decomposition. From the point of view of vote analysis, filamentous structures are characterized by an unbalanced distribution of elements along one main direction. In contrast to other structures whose tensors tend to deform more evenly due to the influence from different directions, curvilinear structures produce elongated tensors. Therefore, tensors from filamentous structures are likely to be evidenced within the stick saliency map (i.e., image formed by computing $\lambda_1 - \lambda_2$ at each location (x, y, z)). Figure 3 (center row) shows the results from enhancement by Hessian followed by detection and completion of filaments by tensor voting. When applying tensor voting, $sigma = 10$ across all images. Curve tracking is then applied so 1-pixel wide filaments can be segmented. Here, $T_{local} = T_{global} = 0.3$ across all images.

Table 1 reports results on the synthetic data assessed by the F_1 Score (i.e., $\frac{2.precision.recall}{precision+recall}$) as a function of m and n.

Table 1. F_1 Score from detection of synthetic helix affected by noisy (n) and missing (m) points.

m \ n	0%	1%	2%	5%	10%
0%	1.0000	1.0000	.9985	.9728	.9680
25%	.9985	.9970	.9985	.9728	.9664
50%	1.0000	1.0000	.9701	.9728	.9610
75%	.9985	.9878	.9728	.9673	.9970
95%	.9970	.9823	.9572	.9807	.9701

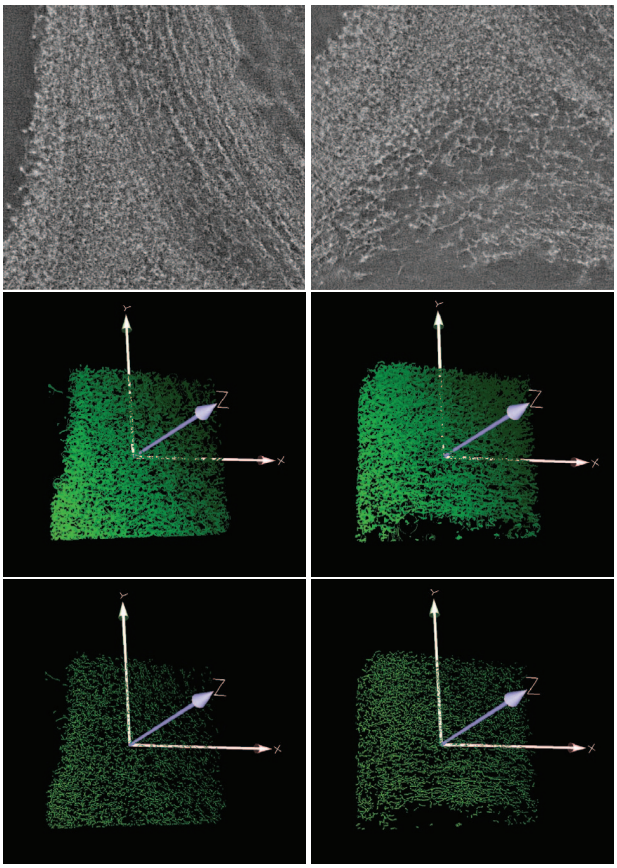


Fig. 3. Tomographic images in our data set (top row), and results produced by tensor voting (middle row) and curve tracking (bottom row).

Figure 3 shows the results produced by our approach on real data. By visually inspecting the results, one can note that they correlate very well with the underlying signal since it tracks the filament's signature along its center.

Detection of polysaccharide filaments allows quantification of the results and estimation of detailed statistics of plant cell wall structure. Figure 4 exemplifies two types of analyses across replicates. Our analyses show that plant cell walls in our data set present a homogeneous aspect both in terms of volume of polysaccharides, occupying between 18% and 28% of the overall volume, and in filament length, with averages varying between 44 and 56 pixels (1 pixel $\cong$ 0.79nm). These findings correlate with our expectations and provide important insight about the structure of the plant cell wall.

4. CONCLUSIONS

This paper presents a computational protocol for automatic detection of filamentous structures imaged by tomographic electron microscopy. Our approach is based on enhancement, detection and delineation of filaments, and leverages the tensor voting framework. Tensor voting inhibits random noise and accentuates structural signature to enable continuity through gap filling and perceptual grouping. The method was applied to real plant cell walls imaged in 3D, resulting in mapping and quantification of polysaccharides. This is a promising approach for quantifying composition of filamentous structures from different species or the same species under different experiment conditions. Ultimately, this method can be utilized for better understanding of the mechanical property of the plant cell wall. We plan to utilize the proposed computational protocol to characterize the composition of plant cell walls as a function of chemical treatments and genetic manipulation.

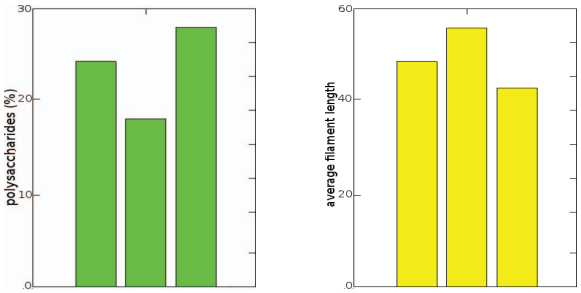


Fig. 4. Quantification of the plant cell wall composition. Left - volume of polysaccharides per replicate (relative to whole imaged volume); Right - average filament length per replicate.

5. REFERENCES

[1] G. Medioni, M.-S. Lee, and C.-K. Tang, "A computational framework for feature extraction and segmentation," Elsevier Science, 2000.

[2] M.C. McCann, B. Wells, and K. Roberts, "Direct visualization of cross-links in the primary plant cell wall," J Cell Science, 1990, vol. 96, pp. 323–334.

[3] K. Sugimoto, R. Williamson, and G. Wasteneys, "New techniques enable comparative analysis of microtubule orientation, wall texture, and growth rate in intact roots of arabidopsis," Plant Physiol., 2000, vol. 124, pp. 1493–1506.

[4] S.Y. Ding and M.E. Himmel, "The maize primary cell wall microfibril: A new model derived from direct visualization," J. Agric. Food Chem, 2006, vol. 54, pp. 597–606.

[5] P. Xu, L.A. Donaldson, Z.R. Gergely, and L.A. Staehelin, "Dual-axis electron tomography: a new approach for investigating the spatial organization of wood cellulose microbrils," Wood Sci. Tech., 2007, vol. 41, pp. 101–116.

[6] A. F. Frangi, "Three-dimensional model-based analysis of vascular and cardiac images," Ph.D. Thesis, Utrecht University, The Netherlands, 2001.

[7] D. N. Mastronarde, "Dual-axis tomography: An approach with alignment methods that preserve resolution," Journal of Structural Biology, 1997, vol. 120, pp. 343–352.

[8] J. R. Kremer, D. N. Mastronarde, and J. R. McIntosh, "Computer visualization of three-dimensional image data using imod," J. of Structural Biology, 1996, vol. 116, pp. 71–76.